ICAST2014 032

Joule Heating of Shape Memory Polymer with Magnetically Aligned Nickel Particles

Richard V Beblo[1*], James J Joo[2], Gregory W Reich[2]

[1] Aerospace Mechanics Division, University of Dayton Research Institute, Dayton, OH, USA
[2] Aerospace Systems Directorate, Air Force Research Laboratory, Dayton, OH, USA

Abstract

One of the major remaining barriers to the widespread adoption of thermally activated shape memory polymer is the method used to heat them. Presented is an investigation into using 5μm Nickel particles aligned into chains as embedded Joule heaters for epoxy shape memory polymer. The high density of particle chain heaters reduces the time and energy required to reach transition by minimizing excess heat required due to the low thermal conductivity of the polymer by heating the material more uniformly. The chains are formed by curing the polymer in a uniform magnetic field generated by two sets of N42SH Neodymium magnets above and below the sample approximately 57 mm apart. Modeling of the induced magnetic field within and between particles during curing and an analytical model predicting particle mobility in a fluid with respect to vibration frequency and amplitude are presented and discussed in context to the current work. Since epoxy resin has a high viscosity, particle mobility is encouraged by sonicating the sample at 300 Hz at an amplitude of approximately 50 μm prior to polymerization using an industrial shaker and Teflon guides. Copper mesh electrodes are attached to the resulting samples using 10% by volume nickel particle SMP epoxy. Significant particle alignment is confirmed via optical microscope images. Electrical resistivity is measured as low as 57 Ω-mm at Nickel volume concentrations of 1.0%. Infrared images of the samples during heating are presented and electrical energy required with respect to sample thermal capacity estimated.

1. INTRODUCTION

Reconfigurable structures have in recent years been the focus of many studies due to their ability to adapt to changing environments as well as their added functionality as compared to their non-reconfigurable counterparts. One such area of research is the design of skins and skin systems capable of large deformations while maintaining structural rigidity in desired directions. Reconfigurable skins have been proposed for a multitude of applications including morphing aircraft, deployable satellites, and shape changing cars. One of the main correlations between these applications is the need for a skin material with controllable, adaptable material properties that offer both structural load bearing capabilities as well

* Richard.Beblo@udri.udayton.edu

as low stiffness configurations during reconfiguration. For this purpose, shape memory polymer (SMP) filled honeycomb cores have been proposed. [1-5]

Honeycomb structures are inherently flexible both in-plane and in bending due to their generally thin walled construction when not paired with face sheets. The structure can be made relatively stiff, however, by filling the voids in the honeycomb with a rigid material effectively resulting in a solid sheet. If the honeycomb is filled with a thermally activated SMP material and each cell heated individually, thus providing cellular level stiffness control, the filled honeycomb composite becomes a stiffness controllable, reconfigurable skin system. Patterns of heated cells, such as those shown in Figure 1, can then be used to alter the macroscopic properties of the material.

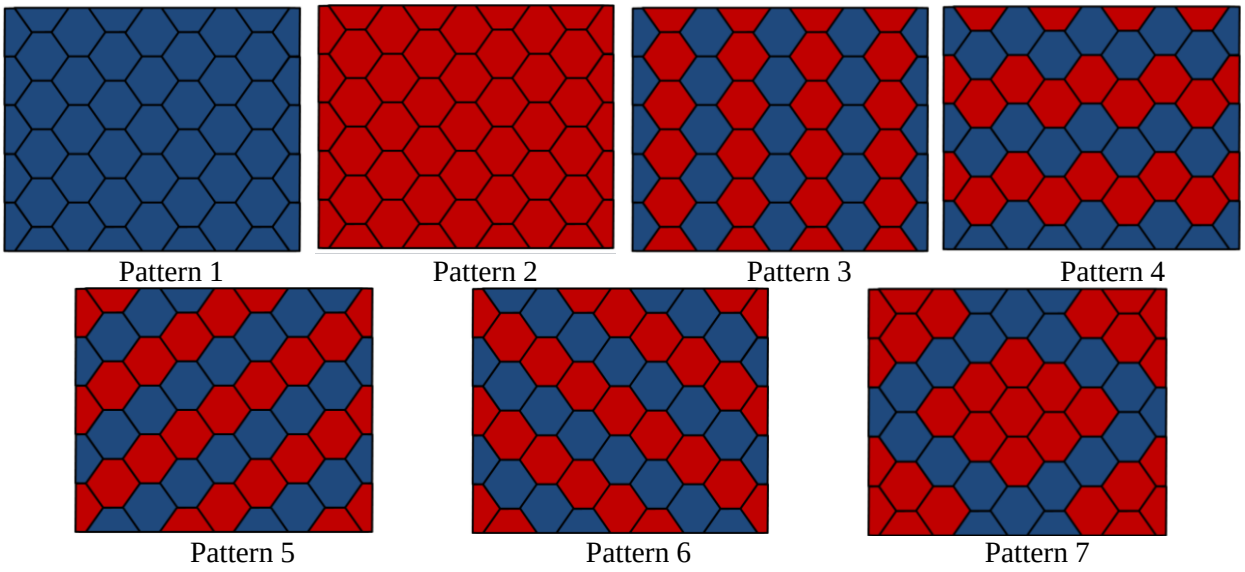

Figure 1. Honeycomb heating patterns

One of the main barriers to implementation of such a skin system is the method used to heat the SMP, which is the focus of the presented work. Methods of making SMPs conductive and thus electrically activated through joule heating have been extensively studied. Systems including carbon fibers, carbon nanotubes, carbon black, exfoliated graphite, metallic nanostrands, metallic powders, small wires, and oxide powders have all been proposed. [6-10] Luo and Mather were able to achieve sub 2 second activation using continuous carbon nanofibers in an epoxy SMP matrix. The T_g for the sample, 50 ºC, was lower than many applications require however and the sample was very thin, whereas transitioning a thick sample is more complicated. Nickel coated graphite fibers [6,7] and stainless steel fibers [7] have been used to create conductive polypropylene composites with some success however require sophisticated manufacturing techniques. Nickel powders have been used similarly to the presented study by Leng et.al, providing joule heating by aligning the particles into chains using lower viscosity resins and a weaker polymer. [8,9] Similar to the presented work, they aligned metallic particles using magnets in a thin strip of uncured polymer resin. The resulting Nickel chains greatly reduced the electrical resistance of the sample and were shown to retain their integrity after several strain cycles.

2. PARTICLE CHAIN SPACING

The SMP used in the current study is an epoxy SMP comprising of EPON826 and JeffamineD230. This polymer was chosen for its known characteristics and tailorable properties. Compositions, cure cycle, and manufacturing procedures are published by Xie et. al. [11] The resistive heating elements embedded in the SMP are constructed of Nickel particles, chosen for their resistive heating, magnetic, and corrosion properties. The particles are approximately 5 μm in diameter spheres supplied by Sigma-Aldrich. Material properties for both the SMP and Nickel particles are shown in Table 1 and Table 2.

Table 1. Nickel Particle Properties

Material Property	**Value**
Density (g/m^3)	8.908e6
Young's Modulus (Pa)	207e9
Electrical Resistivity (Ω-cm)	6.4e-6
Magnetic Permeability	1240
Particle Diameter (m)	5e-6
Thermal Capacity (J/m^3/C)	0.46
Thermal Conductivity (W/m/K)	60.7

Table 2. Shape Memory Polymer Properties

Material Property	**<Tg**	**>Tg**
Young's Modulus (Pa)	1.3e9	1.9e7
Thermal Conductivity (W/m/K)	0.206	0.234
Thermal Capacity (J/m^3/K)	1.43e6	2.45e6
Density (g/m^3)	1.153e6	
Glass Transition Temperature (C)	78	
Viscosity 25C (Pa-s)	8	
Viscosity 75C (Pa-s)	0.08	
Thermal Expansion Coefficient (m/m/K)	55e-6	

Some of the advantages of the chosen heating scheme are its inherent flexibility in material selection, ease of manufacturability, and tailorable properties. Since the polymer has a relatively low thermal diffusivity, either extremely long times are required to heat the polymer to transition or the material nearest the heat source will be significantly above T_g; both of which are undesirable. One of the principal advantages of distributed heat sources such as the presented Nickel particle chains is the excess thermal energy required to heat the polymer quickly is mitigated by minimizing the distance between heat sources.

Using a simple 1D thermal model the minimum volume density of particles needed to heat the SMP to T_g in a given time can be calculated. Particle chains are modeled as cylinders with effective radii based on surface area, *r* in Figure 2. If the chains are efficiently packed in the material and spaced *2b* apart, then each chain is approximately responsible for heating a cylindrical area of radius *b'* from the center of the chain. The SMP is then modeled as a hollow cylinder with inner radius *r* and outer radius *b'*. The outer radius is assumed to be adiabatic due to symmetry while a uniform heat flux, q_{in}, is applied to the inner radius. The cylinder is assumed to be at uniform initial temperature and thermal properties of the polymer are allowed to vary with temperature, see Beblo et al [13]. With an initial temperature of 25 ºC and the temperature at the interface between the chain and polymer limited to 200 ºC to prevent damage to the polymer, the time required for the temperature *b'* from the center of the chain to reach T_g is calculated. Supplied power is distributed over a cube of SMP 1 cm by 1 cm in area and 5 mm thick.

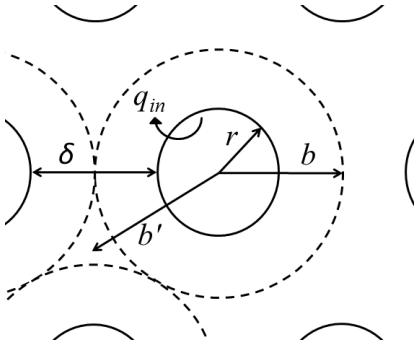

Figure 2. Parameters for 1D thermal diffusion between chains

Figure 4 shows the time required for the temperature *b'* from the particle chain to reach 78 ºC with respect to the volume fraction of Nickel particles. An order of magnitude increase in the volume fraction of Nickel particles results in only a 12% reduction in heating time. Interestingly, the low thermal conductivity of the polymer and limiting the temperature at the interface to prevent damage results in the peak supplied power having little effect on the excess energy required to reach transition, thus only one curve is visible in Figure 4. Excess energy being defined as the amount of thermal energy delivered to the polymer beyond what would be required if the polymer were uniformly at T_g. In each case the temperature of the polymer near the particle chain reaches 200 ºC before the temperature at *b'* reaches T_g. This results in the amount of excess thermal energy required having a similar trend to that of the time required for transition with approximately 13% less energy being required using 10 vol% Nickel than 1 vol% while the peak supplied power has little to no effect.

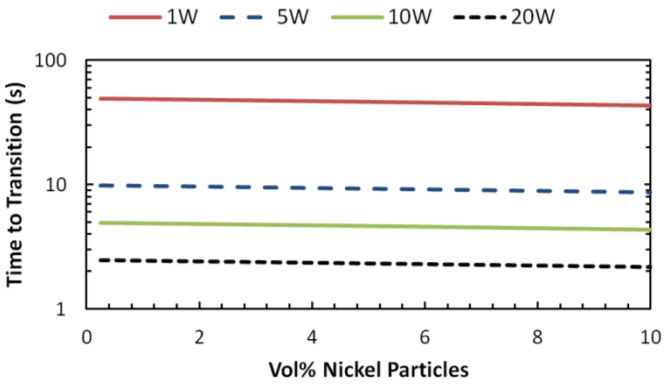

Figure 3. Minimum time to reach T_g given volume fraction of particles and heating power

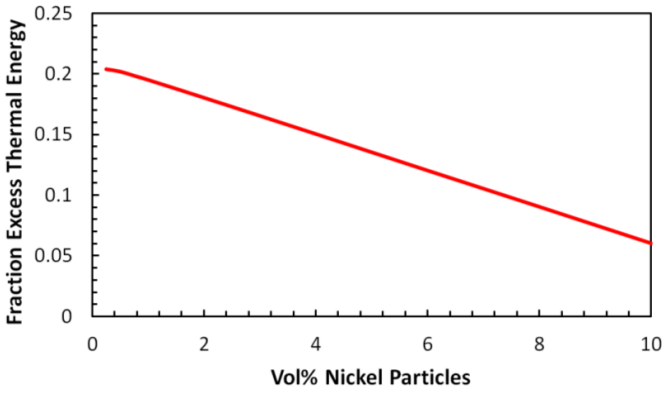

Figure 4. Excess energy required to reach T_g given volume fraction of Nickel particles

A system with perfectly dispersed chains is of course unrealistic. The chains formed in a real system are not evenly spaced, have non-connecting branches and sections, and may be more than one particle in thickness. Thus, the above predictions represent the minimum power and particle fraction required for a desired heating time.

3. EXPERIMENTAL SETUP

3.1 Magnetic Forces

To align the particles into chains, randomly dispersed particles in uncured SMP resin are subjected to a magnetic field. Neodymium N42SH magnets, serviceable up to 150 ºC, encased in aluminum fixtures are suspended above and below the sample as shown in Figure 5 (Left) and Figure 10. The magnets are 60 mm apart with the sample placed in the center. Each magnet is 101.6 mm wide and 3.175 mm thick. The sample shown is 127 mm in length and 5mm thick. The polymer resin sample is in an open Teflon® mold which sits in two "C" shaped Teflon® guide blocks. The magnetic field surrounding the sample is modeled using the freeware program Finite Element Method Magnetics (FEMM) version 4.2. The magnetic field within the sample has an average strength of 4.77e4 A/m, with a standard deviation of 1.9e4 A/m (40%). While there is variation in magnetic field strength horizontally, particularly near the edges, vertically the field is nearly uniform with a standard deviation of 1.82e3 A/m (3.8%). Placing the magnets closer together increases the vertical standard deviation of field strength making the field less uniform. A non-uniform field causes a net non-zero magnetic force between the particles in the sample and the magnets which causes the particles to collect on the top and bottom surface rather than form chains.

Also shown is the magnetic field between three vertically aligned Ni particles. The magnetic polarization created in the particles dramatically increases the field density between nearby particles. The three particles shown in Figure 5 are 5 μm and 15 μm apart. The magnetic polarization created in the particles by the magnets causes the particles to be attracted to one another when aligned vertically; forming chains along the magnetic field lines between the two magnets. The entire assembly is then placed in an oven for curing, ensuring good particle alignment during the expansion and shrinking that occurs during curing.

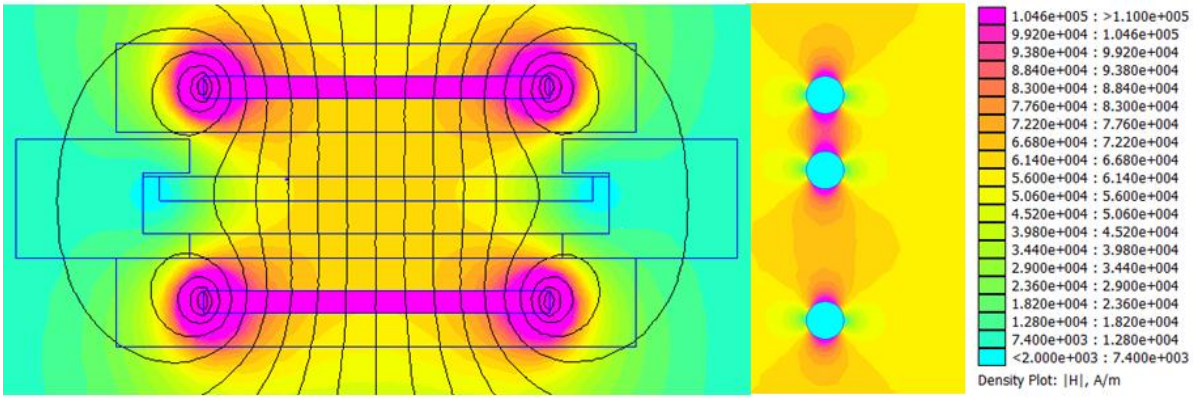

Figure 5. Magnetic field intensity surrounding the sample (Left) and between particles (Right)

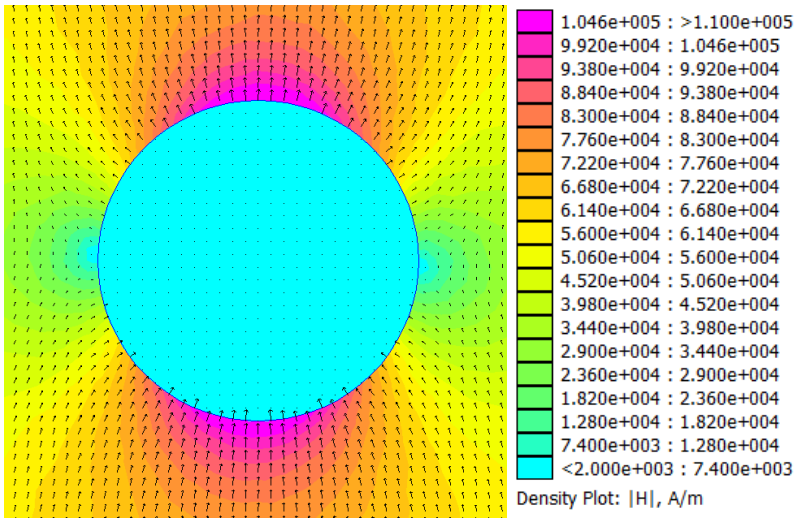

Figure 6. Magnetic field intensity and direction near a Nickel particle

Using FEMM, the attractive or repulsive force exerted on a pair of particles can be calculated. Particles aligned vertically attract while particles in the same plane aligned horizontally repel. The magnetically induced attractive force between two vertically aligned spherical Nickel particles is shown in Figure 7 as a function of the distance between the particles. A similar negative curve can be generated for the repulsive force between particles in plane.

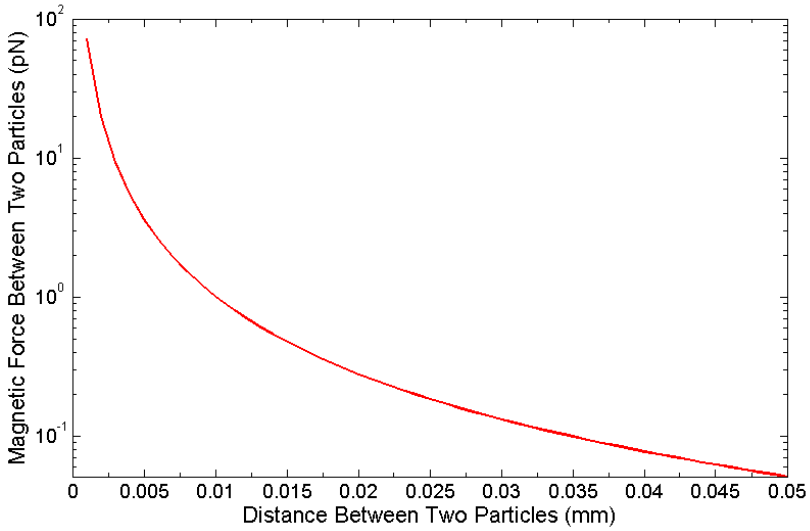

Figure 7. Magnetic attractive force between vertically aligned particles

The net downward force on a particle taking into account gravity and buoyancy is 4.97 pN. Thus, for any positive vertical movement the magnetic force on a particle must be higher than 4.97 pN. With the above magnetic setup this occurs only for particles less than 4.2 μm apart. At 1 vol%, if the particles are efficiently dispersed there is an average 19 μm between each particle. At 19 μm, the magnetic force between two vertically aligned particles is 0.31 pN, far less than is required. While the magnetic field is sufficient to vertically align particles in close proximity, it is insufficient to properly attract particles more than a diameter apart.

It is possible to increase the strength of the magnetic field and thus the induced magnetic field within each particle resulting in stronger magnetic forces between particles. The distance between the magnets pictured in Figure 5 can be decreased or the strength of the magnets can be increased. Either of these methods however would increase the magnetic field gradient experienced by the sample. A strong gradient results in a net non-zero magnetic force between the particles and magnets attracting the particles to either the top or bottom surface of the sample. While not directly studied, increased particle densities near the surface of the sample and significant surface texturing were seen for magnet spacings less than 40 mm apart.

3.2 Vibration Forces

To supplement the force on the particles generated by the magnetic field, linear polarized vibration is introduced to the sample to increase particle mobility. Particle motion in a vibrating fluid has been extensively studied and modelled. [12] Figure 8 shows the direction of forces generated on a particle for any pair of particles aligned along one of the three cardinal axis when subjected to a polarized vibrating fluid.

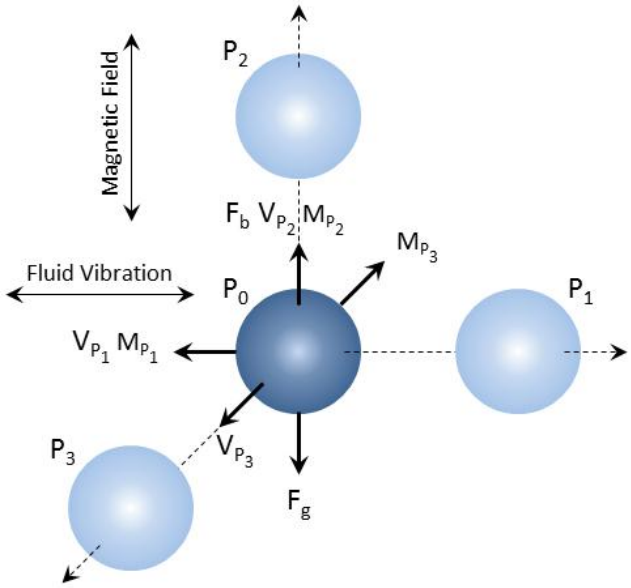

Figure 8. Gravity, buoyancy, vibration, and magnetic forces on a suspended particle

In Figure 8 F_b is the buoyancy force, F_g is the force due to gravity, and V and M are forces induced by vibration and the magnetic field respectively with respect to the nearby particle noted in the subscript. Tangential vibratory forces such as that created between particles P_0 and P_1cause neighboring particles to repel while normal vibrations such as that between P_0 and P_2 cause particles to attract. If the central particle P_0 were surrounded by particles on the negative axes as well as the particles shown in Figure 8 (six particles total) and each were the same size, shape, and distance from particle P_0, the resulting forces due to the vibrating fluid and magnetic field would cancel and the net force on the particle would simply be the difference between the force due to gravity and the buoyancy force. A perfectly uniform distribution of particles would then result in the particles simply settling. Non-uniform particle shape and size and varying distances between particles result in net non-zero force on each particle causing them to preferentially align along magnetic field lines. Since all forces in-plane cause particles to repel, the distribution of chains is nearly uniform.

Lyubimov et. al. derived the below equations for the force experienced by a pair of particles in a vibrating fluid dependent upon their orientation with respect to the vibration.

$$\nabla\bar{v}^2 = 3a^2\omega^2 r^3 \frac{\rho_p - \rho_f}{\rho_f + 2\rho_p}\left(\frac{5\cos^2\theta - 1}{\delta^4}\vec{\tau} - 2\frac{\cos\theta}{\delta^4}\vec{j}\right) \tag{1}$$

$$\vec{F} = \frac{3}{4}V_p\rho_f \frac{\rho_p - \rho_f}{\rho_p + \frac{1}{2}\rho_f}\nabla\bar{v}^2 \tag{2}$$

Where a and ω are the vibration amplitude and frequency, r is the particle radius, ρ_p is the particle density, ρ_f is the fluid density, V_p is the particle volume, δ is the distance between the two particles, $\vec{\tau}$ is a unit normal vector connecting the two particles, $\nabla\bar{v}^2$ is the gradient of the mean squared pulsational velocity averaged over the vibration period, $\vec{j} \bullet \vec{\tau} = \cos\theta$, and $\vec{F}$ is the force experienced on each particle. Particles normal to the flow ($\theta = \pi/2$) experience an attractive force while particles aligned parallel to the flow ($\theta = 0$) repel. Equations 1 and 2 are as of yet unverified for vibrational amplitudes larger than the diameter of the particles being modelled and thus are provided here as a qualitative

reference. It should be noted however that the 50μm 300Hz vibration is applied to the mold. No attempt to measure the motion of the fluid was performed and indeed areas near mold walls exhibit more significant banding than those far from mold walls.

As predicted by Equations 1 and 2, particles normal to the flow experience positive force causing them to attract while the magnetic forces and forces due to parallel flow cause particles to repel. This interplay between attractive and repulsive forces in plane causes banding to occur in the sample where parallel rows of particles accumulate perpendicular to the direction of vibration. This alignment of particle chains can be seen experimentally as shown in Figure 9.

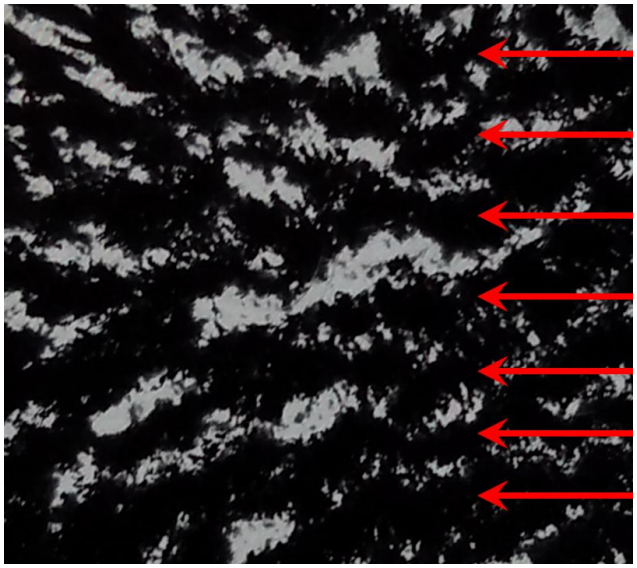

Figure 9. Backlit 10mm thick sample. Particles are dark with a light background. Distinct banding spaced approximately 1mm apart is highlighted with red arrows. Sample subjected to both the magnetic field pictured in Figure 5 and 50μm vibration at 300Hz.

3.3 Sample Fabrication

The experimental setup used to achieve particle alignment is shown in Figure 10. The 300 Hz shaker motor signal is generated by a function generator. The fulcrum connecting the shaker and the mold reduces the stroke of the shaker 10:1 resulting in the sample experiencing an amplitude of approximately 50 μm. After curing, samples are lightly sanded and copper mesh electrodes are applied to the top and bottom surface using the same epoxy SMP with 10 vol% nickel particles. The electrodes are clamped between two thin sheets of Teflon and aluminum plates during curing ensuring good contact.

Figure 10. Experimental magnetic and vibration setup

6. EXPERIMENTAL RESULTS

6.1 Particle Alignment

Using the above method, nickel particle chains can be readily formed in epoxy resin during curing. The magnetic and vibratory forces are sufficient to generate particle motion such that no delay is required between mixing and curing the sample. The particles align in the oven during the first few minutes of the cure cycle before any significant polymerization. Figure 11 shows the alignment achieved in a typical sample. While there are several chains that terminate in the middle of the sample and the chains vary in thickness, there is generally good alignment and distribution.

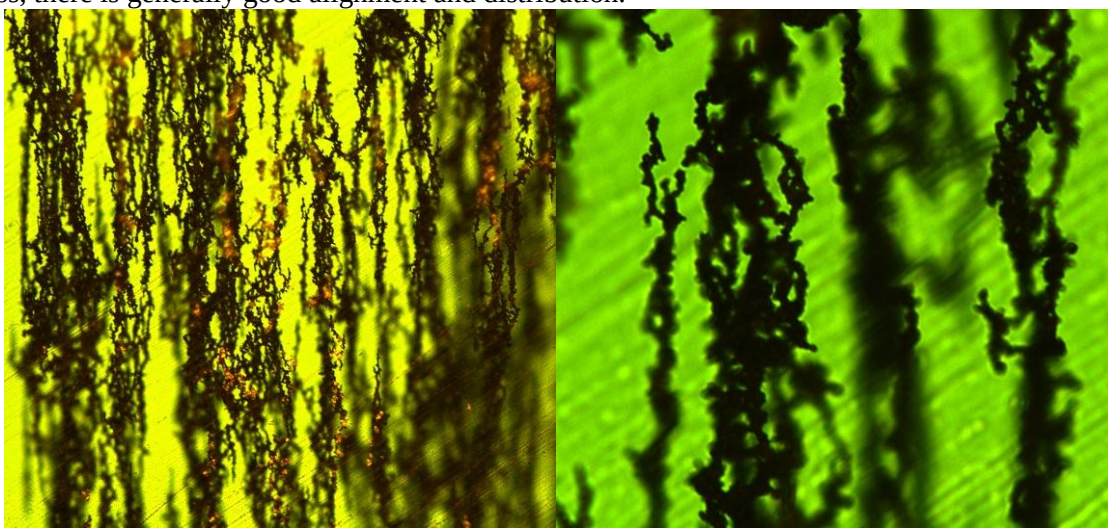

Figure 11. 10X (Left) and 50X (Right) view of Nickel particle chains

6.2 Electrical Properties

As a measure of the quality of particle alignment and the heating capability of the nickel chains, the resistance of 12 samples at various temperatures was measured and the resistivity of the material calculated, Figure 12. At ambient temperature the average resistivity is 57 Ω-mm with very little variation between samples. As the temperature increases the resistivity of the samples increases until unreadably high resistance values are attained above 160 C.

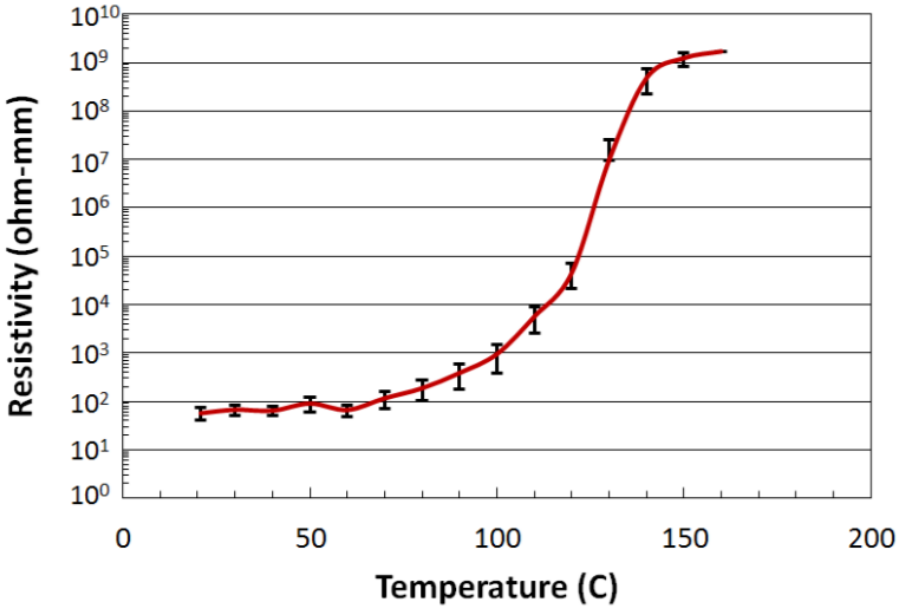

Figure 12. Average resistivity and standard deviation of 12 samples allowed to thermally expand

The more than seven order of magnitude increase in resistivity can possibly be attributed to several factors, the most likely being thermal expansion. Between ambient and 160 C the samples expand by approximately 0.8%. It is postulated that this is sufficient for the majority of particles to be pulled away from one another and cease to physically touch resulting in an open circuit. Indeed, if a sample is placed in a vise in an over at 120 C and gradually subjected to compressive strains the resistivity of the samples reduces to ambient temperature levels as shown in Figure 13.

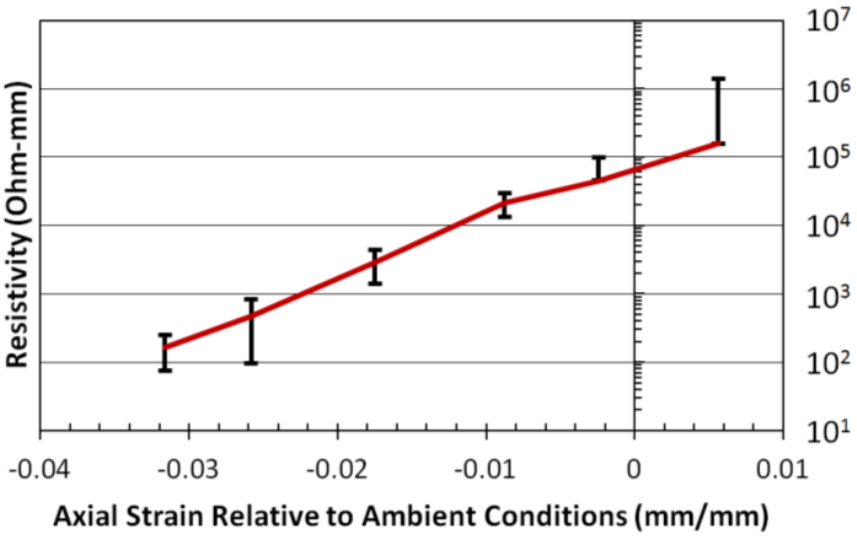

Figure 13. Average resistivity of samples at 120 C subjected to compressive strain

6.3 Thermal Distribution

Regardless of the cause, the increase in resistivity results in two advantages. Due to the variation in the quality and distribution of the Nickel particle chains the samples are not perfectly uniform in their electrical properties. There exist pathways that are more conductive than others through the sample, causing current to preferentially flow through certain chains and not others. If unaltered, this would cause the samples to heat up non-uniformly drastically increasing the time required to reach transition. Since the resistance of the sample increases with temperature (and local thermal expansion), areas of high temperature have higher resistance than those of lower temperature. As current flows through a certain chain or set of chains, the temperature increases. As the resistance increases with increasing temperature the path of least resistance shifts to another area. As current begins to flow through this new area the temperature increases and the cycle continues. This results in the sample heating more evenly and quickly. This can clearly be seen in the series of infra-red images in Figure 14. The left image shows the sample just after current has been turned on where the left most particle chain is slightly warmer than the surrounding sample. After half a second, the temperature of the chain is high enough such that the path of least resistance has moved to the right, Figure 14 middle. Figure 15 shows a magnified section of the sample shown in Figure 14 overlaid with an optical image of the sample. Areas of increased temperature clearly align with areas with a high density of particle chains.

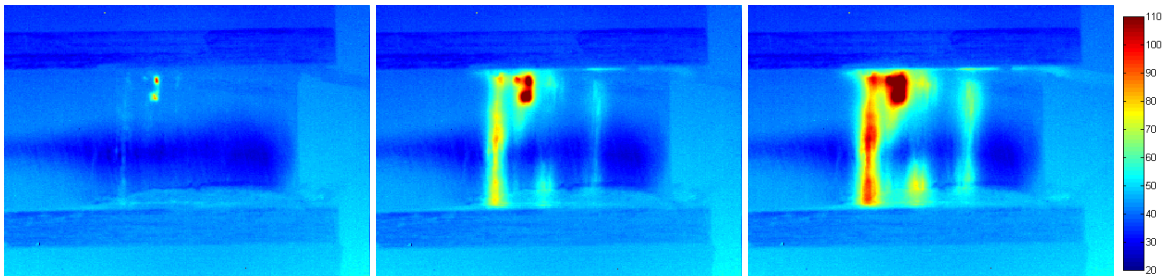

Figure 14. Infrared images of 30V, 0.01A applied to 8mm tall by 2mm thick sample. 0.055s (Left), 0.55s (Middle), and 0.935s (Right) (°C)

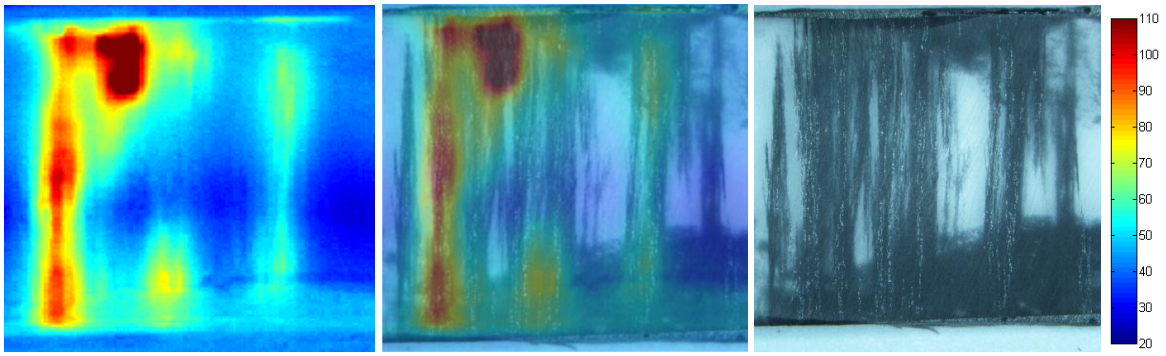

Figure 15. Infrared (Left), optical (Right), and overlay (Middle) images of Nickel chain heating (°C)

The second advantage is the ability to use the resistance of the sample as a temperature sensor. Rather than requiring a separate thermocouple to determine when the transition temperature has been reached, the resistance of the sample can be used to estimate temperature.

6.4 Energy Performance

To demonstrate the functionality of the system, samples similar to those pictured in Figure 1 are connected to several National Instruments NI-9481 switch modules controlled by LabView® and a voltage source. It is desired to supply samples with as much power as possible resulting in the quickest possible heating times. To prevent damage to the modules, voltage and current are limited to 41.8V and 3.1A. At low resistance values, current limits the amount of power than can be supplied to the sample. At high resistance values voltage limits the power that can be supplied to the sample. Peak power is attained when both voltage and current are at their maximum allowable values when the sample has a resistance of 13.5 Ω, Figure 16.

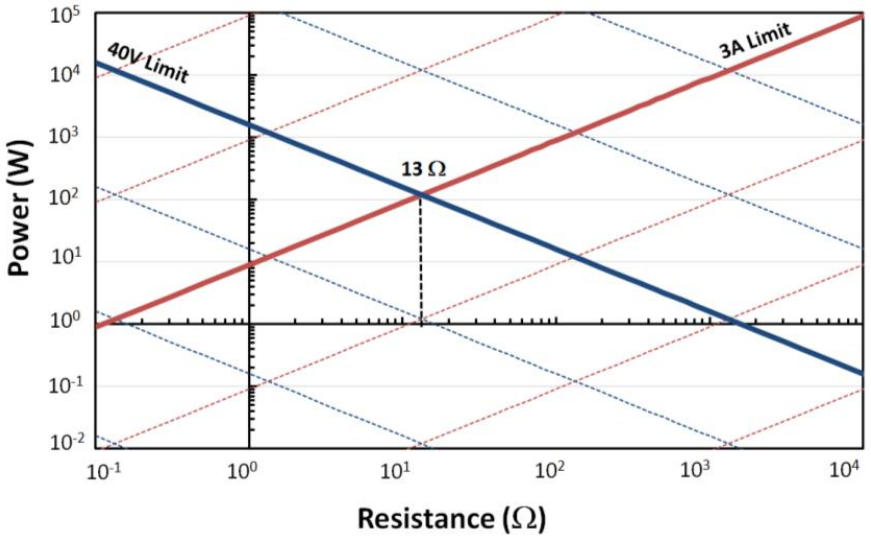

Figure 16. Power supplied to the sample given current and voltage limitations. Iso-voltage and current lines are plotted against sample resistance with 40V and 3A highlighted.

Experimentally, the voltage and current can be continuously varied to deliver maximum power to the sample. When the voltage and current reach levels predetermined to correspond to a sufficiently high resistance indicating the sample has reached T_g, the current is turned off. For the example case shown in Figure 17, current is applied to a row of cells similar to Pattern 4 in Figure 1. Initially, maximum power is achieved by maximizing the current with a low voltage. As the temperature and resistance of the sample increase, the voltage increases until the limit of the voltage source is reached at 37 seconds at which point the current begins to decrease. When the current reaches 0.4 amps at 84 seconds, power is transferred to the row two rows above the first.

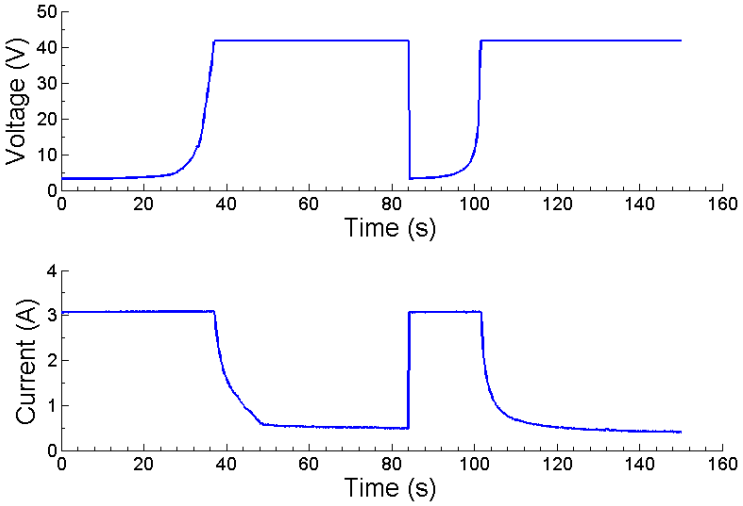

Figure 17. Demonstration of using increase in resistance to estimate temperature

The total electrical power delivered to first row is 2125 J while 1523 J is delivered to the second row. The difference is likely attributable to differences in the quality of particle alignment or contact with the electrodes. Theoretically, increasing the temperature from ambient to 80 C of samples 16.4 cm^2 and 6.6 mm thick should require only 907 J. From previous calculations, if 20% (181 J) of the excess energy can be attributed to the volume fraction of particles, Figure 4, the remaining 1037 J (49%) for the first row and 435 J (29%) for the second row is due to less than ideal particle chains. It should be noted that the 10.8 cm^3 rows used here are significantly larger than the 0.5 cm^3 samples used in the analysis in Section 2.

7. CONCLUSIONS

A method for aligning magnetic particles in fluids with high viscosities has been demonstrated leading to an effective technique for quickly and uniformly heating shape memory polymer. It has been shown that sub-two second activation times are achievable with very low volume fractions (<1.0%) of conductive particles minimizing the added weight associated with many heating methods. The low volume fractions are made possible by aligning nickel particles into chains under a magnetic field and polarized vibration. The requirement that the particles be magnetic however limits the selection of particle materials and precludes traditional dopants such as carbon black. Such dopants could however be used to increase the diffusivity of the composite, further reducing the transition time by decreasing the non-uniform temperature distribution. The composite's increase in resistivity with increasing temperature was characterized and utilized experimentally to aid in uniformly heating and sample and as a thermoelectric switch signaling when the sample had reached the transition temperature. Significant differences in the time and power required to reach transition were measured and are believed to be due to variations in the

quality of particle alignment within the samples. With optimization of manufacturing techniques the excess energy required over the thermal capacity of the polymer should be able to be reduced, making the presented heating method even more attractive for applications. The presented SMP heating method adds minimal additional weight, is simple to manufacture, results in uncomplicated designs, is low cost, and results in uniform temperature making it ideal for many shape memory polymer applications.

ACKNOWLEDGMENTS

Financial support by Dr. Les Lee at AFOSR and assistance in conducting the experimental work by Brian Smyers and Catherine Becker is graciously acknowledged. Cleared for public release, case 88ABW-2014-4396.

REFERENCES

1. Thill, C., Etches, J., Bond, I., Potter, K., and Weaver, P., "Morphing Skins – A review", *The Aeronautical Journal*, vol. 112, 2008, pp. 117-138.
2. Murray, G., Gandhi, F., and Hayden, E., "Polymer Filled Honeycombs to Achieve a Structural Material with Appreciable Damping", *50th AIAA Structures, Structural Dynamics, and Materials Conference*, AIAA2009-2119, Palm Springs, CA, 2009, pp 1-18
3. Henry, C., and McKnight, G., "Cellular variable stiffness materials for ultra-large reversible deformations in reconfigurable structures", *Proceedings of SPIE*, vol. 6170, 2006
4. Olympio, R., and Gandhi, F., "Flexible Skins for Morphing Aircraft Using Cellular Honeycomb Cores", *Journal of Intelligent Material Systems and Structures*, vol. 21, no. 17, pp 1719-1735, 2010
5. Joo, J., Reich, G., and Westfall, J., "Flexible Skin Development for Morphing Aircraft Applications via Topology Optimization", *Journal of Intelligent Material Systems and Structures*, vol. 20, no. 16, pp 1969-1986, 2009
6. Weber, M., and Kamal, M., "Estimation of the Volume Resistivity of Electrically Conductive Composites", *Polymer Composites*, vol. 18, no. 6, 1997
7. Weber, M., and Kamal, M., "Microstructure and Volume Resistivity of Composites of Isotactic Polypropylene Reinforced with Electrically Conductive Fibers", *Polymer Composites*, vol. 18, no. 6, 1997
8. Leng, J., Huang, W., Lan, X., Liu, Y., and Du, S., "Significantly reducing electrical resistivity by forming conductive Ni chains in a polyurethane shape memory polymer/carbon black composite", *Applied Physics Letters – American Institute of Physics*, vol. 92, 2008
9. Leng, J., Lan, X., Liu, Y., Du, S., Huang, W., Liu, N., Phee, S., and Yuan, Q., "Electrical conductivity of thermoresponsive shape memory polymer with embedded micron sized Ni powder chains", *Applied Physics Letters – American Institute of Physics*, vol. 92, 2008
10. Kujawski, M., Pearse, J.D., Smela, E., "Elastomers filled with exfoliated graphite as compliant electrodes", *Carbon*, vol. 48, pp 2409-2417, 2010
11. Xie, T., and Rousseau, I., "Facile tailoring of thermal temperatures of epoxy shape memory polymers", *Polymer*, vol. 50, pp 1852-1856, 2009
12. Lyubimov, D. V., Baydin, A. Y., Lyubimova, T. P., "Particle Dynamics in a Fluid Under High Frequency Vibrations of Linear Polarization", *Microgravity Sci. Technol.*, vol. 25, pp 121-126, 2013
13. Beblo, R., Joo, J., Smyers, B., Reich, G., "Thermal Properties of Magnetite Nanoparticles and Carbon Fiber Doped Epoxy Shape Memory Polymer", ASME Conference on Smart Materials Adaptive Structures and Intelligent Systems, Phoenix, AZ, Sept 18 – Oct 1, 2011